Gao et al. SUPPLEMENTAL INFORMATION

Genomic analysis of P493 cells and xenografts, and the anti-tumorigenic effects of NAC

The dramatic effect of NAC on P493 tumorigenesis (Figures 1A and 1B) led us to determine whether the dominant effect of NAC resulted from reduced genomic instability via reduction of ROS and γH2AX by NAC (Figures S1A-1C). Hence, we compared the genomes of P493 cell lines with those P493 cells recovered from xenografts by G-banding and spectral karyotyping (Figure S1D) as well as high density SNP analysis (Figure S1E) and array CGH (Figure S1F). The cell lines and cells recovered from xenografts are indistinguishable by these state-of-the-art genome analyses, indicating that the human P493 cell line's MYC-dependent tumorigenic potential is not associated with the dramatic chromosomal instability. Hence, the dominant anti-tumorigenic effect of NAC could not be due to the reduction of genomic instability. In fact, human Burkitt's lymphoma, which is modeled by the P493 system, is associated with much fewer genomic changes than the comparably aggressive human diffuse large B cell lymphomas (Hummel et al., 2006). In addition, it is notable that in contrast to bona fide human Burkitt lymphoma cell lines, such as Ramos, that only requires 500,000 cells to establish tumors in SCID mice (data not shown), the P493 cells require 20-30 million cells. Hence, while MYC is necessary for tumorigenesis, the tumorigenic potential of the P493 cells is low, attesting to the lack of extensive mutations already present for efficient tumorigenesis. We have selected this model specifically because it is inefficient in tumorigenesis and hence provides an opportunity to study tumor progression and genomic instability.

Our observations indicate that although clonal selection appears to occur for P493 tumorigenesis, no global genomic changes were detected. Thus, it is very unlikely that NAC inhibits tumorigenesis primarily through reducing DNA damage or genomic instability. Moreover, if ROS were to damage DNA and cause a 'hit-and-run' effect that is dominant, then NAC should not have an in vivo anti-tumorigenic effect that is dominantly dependent on HIF1α, as demonstrated especially by the

rescue experiments using the CA5 cell lines (Figures 4, 5 and 7). We have in fact found that NAC anti-tumorigenic effect is negated by CA5 in MYC-dependent P493 and MYC-independent PC3 tumors. These observations taken together indicate that the dominant anti-tumorigenic effect of anti-oxidants involve HIF-1α and not genomic instability.

Reference

Hummel, M., Bentink, S., Berger, H., Klapper, W., Wessendorf, S., Barth, T. F., Bernd, H. W., Cogliatti, S. B., Dierlamm, J., Feller, A. C*., et al.* (2006). A biologic definition of Burkitt's lymphoma from transcriptional and genomic profiling. N Engl J Med *354*, 2419-2430.

Supplemental Figures

Figure S1. A. Myc induction in P493 B cells is associated with increased phosphorylated histone H2A.X (γH2AX), a surrogate marker of double stranded DNA breaks. **B.** N-acetylcysteine (NAC) reduces γH2AX induced by Myc in P493 cells. P493 cells were grown in log phase in the absence of tetracycline (Tet -) or in the presence of Tet (+) for 48 hr, with or without N-acetylcysteine (NAC; 10 mM). Tet treated cells were washed to induce Myc and samples were obtained at 16 hr and 24 hr after removal of Tet. Cell lysates were obtained for immunoblotting to determine the levels of Myc, γH2AX or tubulin that serves as a loading control. **C.** Flow cytometric determination of ROS production measured by CM-H2DCFDA fluorescence as a function of MYC status (*upper left*) and the presence or absence of N-acetylcysteine (NAC; 10 mM). The presence of tetracycline inhibits MYC expression in P493 cells (-MYC) and conversely the absence of tetracycline induces MYC (+MYC). The effect of NAC on ROS production is shown for +MYC and –MYC conditions (*upper right and lower left*). The composite of the histograms are shown (*lower right*). **D.** Representative spectral karyotypes of P493 cells grown in vitro and those (lower panel) recovered from xenografts in SCID mice. A ring

chromosome 6 is identified. Note that a loss of the trisomic chromosome 9 is seen in <10% cells from xenografts. **E.** Illumina HumanHap300 BeadChip data for chromosome 16 displayed by Genome Viewer software. Chromosome 16 bands are depicted at the top with the first panel showing heterozygosity of 16p (AB allele) and LOH of 16q (AA or BB alleles). The lower panel represents copy number of the SNPs relative to control. Note a region of loss in 16q12.1 and normal copy number LOH for the remaining 16q. Survey of all chromosomes showed no significant differences between in vitro cultured P493 cells and those recovered from xenografts. **F**. Agilent Array CGH comparing two parental (P1 vs P2) P493 cell lines, Tumor 1 (T1) vs P2 and Tumor 2 (T2) vs P2. Note that the signals could not distinguish between parental and tumor cells. Microarrays were scanned with Agilent G2565BA microarray scanner under default settings recommended by Agilent Technologies for array CGH with 100% PMT and 10 um resolutions. Data were extracted using Feature Extraction Software v8.1 (Agilent Technologies) under default settings for array CGH. SNP and CGH raw data are available in the Gene Expression Omnibus (GEO) database; GEO accession GSE8627.

Figure S2. A. Immunoblot of HIF2α in normoxic or hypoxic P493 cells or RCC4+VHL cells untreated or treated with N-acetylcysteine (NAC; 10 mM). Note that HIF2α protein is undetectable in P493 cells and its presence in hypoxic RCC4-VHL cells is diminished by NAC. Tubulin serves as loading control. **B.** HIF2α mRNA determined by real-time PCR and normalized to 18S RNA is undetectable in P493 cells as compared with RCC4 cells. Data are shown as mean ± SD.

Figure S3. Induction of HIF1α in P493 cells treated with siRNA against prolyl hydroxylase 2 (PHD2) is not diminished by N-acetylcysteine (NAC; 10 mM). P493 cells were treated with control siRNA or siRNAs targeting either PHD1 or PHD2 and then exposed to NAC. Immunoblots for HIF1α, PHD1, PHD2 and tubulin are shown.

Supplemental Text and Figures

Figure S1

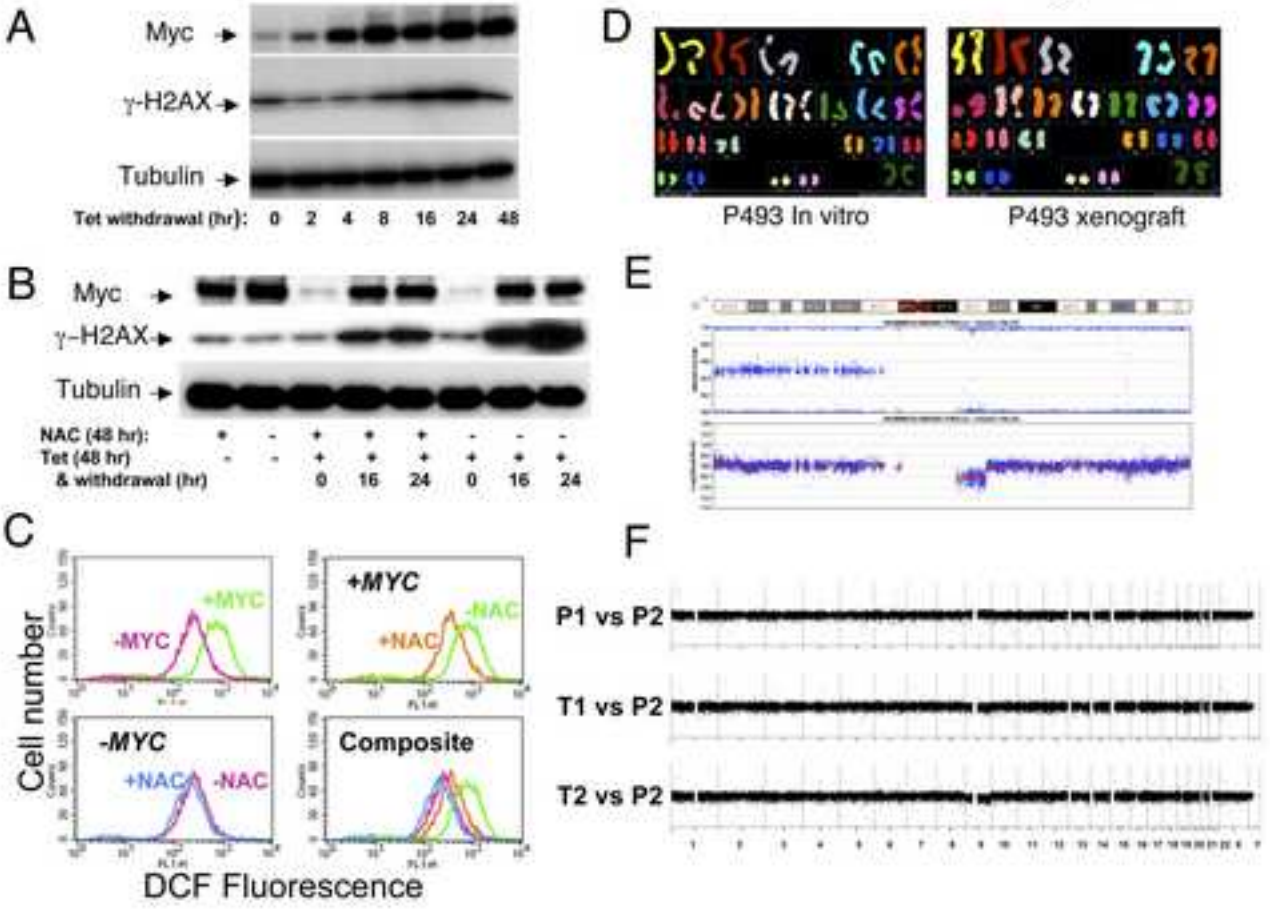

Figure S2

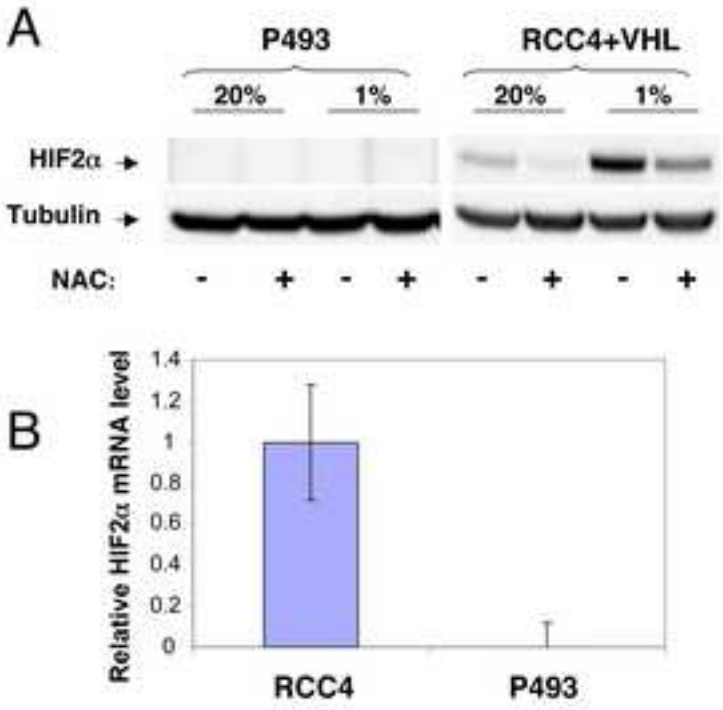
A
P493
RCC4+VHL
20%
1%
20%
1%
HIF2α
Tubulin
NAC:
- + - + - + - +
B
Relative HIF2α mRNA level
1.4
1.2
1
0.8
0.6
0.4
0.2
0
RCC4
P493

Figure S3